Self-Consistent Electrothermal Modeling of Passive and Microchannel Cooling in AlGaN/GaN HEMTs

Man Prakash Gupta, Ajit Kumar Vallabhaneni, and Satish Kumar

***Abstract*— AlGaN/GaN high electronic mobility transistors (HEMTs) are highly promising for power and RF electronics due to large bandgap and high breakdown voltage. However, the thermal bottlenecks associated with the elevated temperatures in the device at high power density presents significant barriers in achieving the full potential of these HEMTs. Embedded cooling solutions have been explored for these devices for the efficient thermal management of extreme heat fluxes and hotspots. This involves conductive, convective, and evaporative cooling methods located closer to the electrically active regions of the device. Developing simulation tools that can guide thermal-mechanical-electrical co-design are necessary for implementation of the embedded cooling solutions. We present self-consistent electrothermal models for AlGaN/GaN HEMTs to study the passive and embedded microchannel cooling. In the case of passive cooling, we develop a fully compact electrothermal model that is computationally very efficient and provides high-fidelity results. The model can capture the spatial variation of temperature profile in the device and can predict the temperature-dependent drain current variation among the various fingers in a multifinger HEMT. We then explore the potential of liquid cooling of a multifinger AlGaN/GaN HEMTs using microchannels embedded in the substrate. A 3-D computational fluid dynamics (CFD) model of the device is coupled with the compact dc current model. Our analysis shows that the self-consistency effects on power and temperature remain significant even for the high flow rates in microchannels. Predictive capability of the "standalone" CFD models of AlGaN/GaN HEMTs can be limited unless they are self-consistently coupled with the electrical models.**

***Index Terms*— Gallium nitride (GaN), high electron mobility transistor (HEMT), microchannel cooling, modeling and simulation, thermal management.**

I. Introduction

AlGaN/GaN-BASED high electron mobility transistors (HEMTs) are considered to be a promising technology for high-power and high-frequency applications. A combination of properties such as high breakdown voltage, large bandgap, high sheet charge, and high saturated drift velocity make it an excellent choice for high-voltage and high-frequency power-electronic applications [2]. The AlGaN/GaN HEMTs-based technology offers great advantages for many industrial applications related with defense, medical, and transportation [2]–[6]. However, the thermal bottlenecks associated with the elevated temperature in the device at high power density present significant barriers in achieving the full potential of the HEMTs. High power density in AlGaN/GaN HEMTs (up to hundreds of watts per die) leads to excessive self-heating, which can significantly affect the device performance and reliability [2], [3]. Hence, efficient heat dissipation in the device is likely to be one of the primary design criteria for the transistor layouts and material selection [1], [7]. Currently, SiC is the most commonly used substrate material in AlGaN/GaN HEMTs due to its high thermal conductivity (∼380 W/m–K at 300 K). Due to cost considerations, Si is also an attractive substrate material for these devices in some applications. However, Si has a lower thermal conductivity (∼148 W/m–K at 300 K) compared to SiC, which translates into greater junction temperature leading to lower performance and poor reliability. While significant efforts are being made to enhance the passive cooling by using high-thermal-conductivity substrate materials such as the diamond, active cooling techniques such as microchannel liquid cooling has also been explored to reduce the temperatures in high-power electronics [8], [9]. With the mandate of DARPA's current ICECool program to develop next-generation thermal management techniques for extreme heat fluxes and hotspots in electronics, highly integrated embedded cooling solutions are being explored for these devices. This involves efficient conductive, convective, and evaporative cooling methods located closer to the electrically active regions of the device.

Chen *et al.* [1] discussed the recent progress in the next-generation thermal management solutions such as embedded cooling of GaN power amplifiers. With the demonstrated passive cooling enhancement from the diamond substrate, resulting in three times more power handling capability for GaN-on-diamond compared to GaN-on-SiC, more progress is anticipated by bringing convective and evaporative cooling much closer to heat generating junction region of GaN HEMTs. Bar-Cohen *et al.* [10] proposed a membrane-based evaporative cooling solution for GaN HEMTs in which coolant gets evaporated in a thin nano-porous membrane supported by a microchannel cooler. They suggested that this evaporative technique can reduce the hot-spot temperature by more than 40 K compared to single-phase microchannel cooling. Lu *et al.* [11] performed computational fluid dynamics (CFD) simulations to explore a microcooler design that can dissipate large heat fluxes (>30 kW/cm^2) in GaN HEMTs while maintaining hot-spot temperature below 250 °C. The microcooler design involves the fabrication

Manuscript received November 11, 2016; revised March 13, 2017; accepted April 1, 2017. Date of publication May 11, 2017; date of current version August 14, 2017. Recommended for publication by Associate Editor F. Shi upon evaluation of reviewers' comments. This work was supported in part by the DARPA Young Faculty Award under Grant N66001-14-1-4050. *(Corresponding author: Man Prakash Gupta.)*

The authors are with the G. W. Woodruff School of Mechanical Engineering, Georgia Institute of Technology, Atlanta, GA 30332 USA (e-mail: mp.gupta@gatech.edu; satish.kumar@me.gatech.edu).

This paper has supplementary downloadable material available at http://ieeexplore.ieee.org, provided by the authors. It contains more details about the coupled electrical and thermal model.

Color versions of one or more of the figures in this paper are available online at http://ieeexplore.ieee.org.

Digital Object Identifier 10.1109/TCPMT.2017.2693399

of microchannels directly on the SiC substrate, which significantly reduces the thermal resistance between the hotspot and the coolant. Lee *et al.* [12] performed simulations for integrated microfluidic cooling located near the junction region of GaN HEMT. They studied the impact of such a cooling mechanism on electrical-mechanical-thermal co-design of GaN HEMT-based monolithic microwave integrated circuits. Using embedded microfluidics cooling, they showed that heat fluxes in excess of 30 kW/cm^2 near the hotspot and 1 kW/cm^2 at die level can be managed with junction temperature within limits to allow reliable operation.

Developing simulations tools that can guide thermal-mechanical-electrical co-design is necessary for implementation of embedded cooling solutions. Most of the previous studies, using CFD models for thermal analysis, have utilized temperature-independent power to examine the thermal behavior of these devices [1], [8], [11], [13], [14]. Since the drain current (and hence the dissipated power) depends on the device temperature and vice versa, it is important that both electrical and thermal simulations be performed self-consistently. This will allow the accurate modeling of the device, which can provide information about not just the current but also the temperature profile in the transistor, considering the effect of flow in the microchannels, which is necessary for reliable co-design [15]–[17].

In this paper, we present a compact *self-consistent* electrothermal model for AlGaN/GaN HEMTs to study both passive and active (microchannel) cooling of these devices. We utilize a physics-based compact drain current model proposed in [18] for AlGaN/GaN HEMT and couple it with CFD-based thermal model. This paper builds upon our previous paper where we developed a self-consistent reduced-order electrothermal model for GaN HEMTs [19]. The physics-based compact drain current model utilized here offers greater predictive abilities over a wide range of operational conditions of the device. We compare and successfully validate the results from the electrothermal model to experiments (for output characteristics) and finite-volume simulations (for temperature) of AlGaN/GaN HEMT on Si substrate.

The main contributions of this paper are as follows: 1) We develop self-consistent electrothermal models for both single- and multifinger GaN HEMTs by combining a physics-based compact dc current model with both 2-D and 3-D thermal models. We use the developed compact 2-D electrothermal model to study the passive cooling in the device. We demonstrate that the predictive capability of the "standalone" thermal models of GaN HEMTs can be very limited unless they are self-consistently coupled with electrical models due to the strong temperature dependence of the electrical current. 2) We couple a 3-D CFD model of the device with the compact dc current model and employ the developed model to explore the potential of near-junction microchannel cooling of a multifinger GaN HEMT when the microchannels are located in the substrate layer of the device itself. Analysis demonstrates that the self-consistency effects on power and temperature become smaller for higher flow rates, but remain significant for the entire range of flow rate considered or needed for the thermal management.

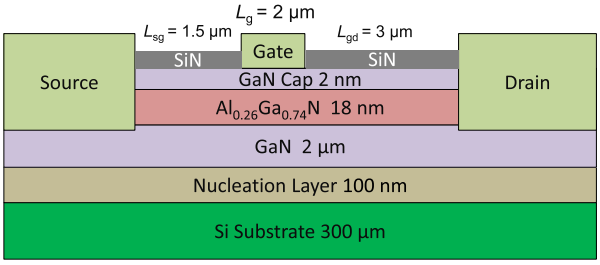

Fig. 1. Schematic of a single-finger AlGaN/GaN HEMT.

This paper is arranged as follows: In Section II, we discuss the methodology used to develop compact electrothermal model for AlGaN/GaN HEMT to simulate current and temperature self-consistently. In Section II-B, we compare results for AlGaN/HEMT obtained from the compact electrothermal model to the experiments and physical simulations to validate the model. Then, in Section III, we include the results and discussion for multifinger AlGaN/GaN HEMT for both passive and microchannel cooling. Finally, we summarize the important contributions of this paper.

II. Methodology

A cross-sectional schematic view of a single-finger AlGaN/GaN HEMT is shown in Fig. 1. The current in the channel region is obtained using an analytical drain current model. The model utilizes a physics-based 2-D electron charge density (2DEG) model valid for different regimes of device operation including near-threshold and subthreshold gate bias conditions [20].

A. Drain Current Model

A simple analytical expression for the drain current is presented below. The derivation of the expression is presented in [20] and [21], but briefly discussed below for completeness. The current in the channel ($I_{\rm ds}$) is specified by (1). Here, q is electron charge, n_s is sheet charge (charge density per unit area), μ is low-field mobility of the device, W is device channel width, L is channel length, V is the local quasi-fermi potential, x is position variable along the channel length, and $V_{\rm s}$ and $V_{\rm d}$ are source and drain voltages

$$I_{\rm ds} = q n_s \mu W \frac{dV}{dx} \Rightarrow I_{\rm ds} = \frac{W}{L}\int_{V_{\rm s}}^{V_{\rm d}} q n_s \mu dV. \quad (1)$$

Using the triangular potential well approximation for 2-D electron gas at the AlGaN/GaN interface, the sheet charge (n_s; charge per unit area) can be specified as a function of the first two subbands energy levels (E_0 and E_1) [22]

$$n_s = D V_{\rm th}[\ln(e^{(E_{\rm f}-E_0)/V_{\rm th}}+1) + \ln(e^{(E_{\rm f}-E_1)/V_{\rm th}}+1)]. \quad (2)$$

Some of the symbols used to denote the parameters are defined in Table I. Subbands (E_0 and E_1) can be specified as

$$E_0 = \gamma_0 n_s^{2/3} \text{ and } E_1 = \gamma_1 n_s^{2/3} \quad (3)$$

where the constants γ_0 and γ_1 adjustable parameters and generally obtained from the experiments [23].

TABLE I
NOTATION OF THE PARAMETERS USED IN THE MODEL

Symbol	Quantity
q	Electron Charge
k_B	Boltzmann constant
T	Temperature
$V_{\text{th}} = k_B\, T/q$	Thermal voltage
ε	Dielectric permittivity of AlGaN
$C_{g=}\, \varepsilon/\, d$	Gate capacitance per unit area
d	Thickness of AlGaN
E_{f}	Fermi energy level
$E_{0,}\, E_1$	First and second energy levels in 2DEG region
D	Density of states

Assuming AlGaN layer to be completely ionized, sheet charge density (n_s) can also be obtained as a function of gate voltage (V_{g}) and Fermi energy level (E_{f})

$$n_s = \frac{\varepsilon}{qd}(V_{\text{g0}} - E_{\text{f}}). \tag{4}$$

Here, $V_{\text{g0}} = V_{\text{gs}} - V_{\text{OFF}}$; V_{OFF} is threshold voltage.

Furthermore, considering only the first energy level (since the second energy level (E_1) is much higher than Fermi energy level (E_{f}) for the range of gate bias used during device operation), and employing (2)–(4) together, we can obtain a relation between sheet charge density (n_s) and local quasi-Fermi potential (V) given by

$$V_{\text{g0}} - V = \frac{qdn_s}{\varepsilon} + \gamma_0 n_s^{2/3} + V_{\text{th}} \ln\left(\frac{n_s}{DV_{\text{th}}}\right). \tag{5}$$

Using (1) and (5), we obtain the drain current (I_{ds}) as a function of charge carrier concentration at source and drain, n_S and n_D, respectively [24]. More details about the derivation of n_S and n_D are provided in the supplementary material

$$I_{\text{ds}} = -\frac{q\mu W}{L}\left[\begin{array}{l}\frac{qd}{2\varepsilon}\left(n_D^2 - n_S^2\right) \\ +\frac{2}{5}\gamma_0\left(n_D^{5/3} - n_S^{5/3}\right) + V_{\text{th}}(n_D - n_S)\end{array}\right]. \tag{6}$$

The low-field mobility model has been utilized in the drain current model [22]. The expression for mobility (μ) is given by (7)

$$\mu = \mu_{\text{min}} + \frac{\mu_{\text{max}} - \mu_{\text{min}}}{1 + \left(\frac{n_s}{n_{\text{ref}}}\right)^{\alpha}} \tag{7}$$

μ_{min}, μ_{max}, n_{ref}, and α are temperature-dependent fitting parameters. The parameter μ_{max} represents the mobility of undoped or unintentionally doped samples, where the main scattering mechanism is lattice scattering. μ_{min} is the mobility in highly doped material, where impurity scattering is dominant. The parameter α is a measure of how quickly the mobility changes from μ_{max} to μ_{min}, and n_{ref} is the carrier concentration at which the mobility is halfway between μ_{max} and μ_{min}. The mobility model takes into account the self-heating effects through the temperature dependence of these parameters provided by

TABLE II
PARAMETERS USED IN MOBILITY MODEL

	μ_{min} (cm^2/Vs)	μ_{max} (cm^2/Vs)	n_{ref} (10^{14}cm^{-2})	α
A_0	100	1000	1	1
ζ_A	-0.85	-1.7	1.3	0.31

$$A(T) = A_0\left(\frac{T}{300}\right)^{\zeta_A}. \tag{8}$$

The values of the parameters specified in (7) and (8) are provided in Table II. It can be noted here that the mobility expression given above is a low-field mobility model, but it works well to simulate the experimental I–V curves for the full range of V_{ds} (0–10 V) considered here. The likely reason is that the peak lateral electric field in the channel is still less than 30 kV/cm corresponding to $V_{\text{ds}} = 10$ V (the channel length is 6.5 μm; gate to drain separation is 3 μm, where most of the potential drop occurs in the channel). For higher electric field, mobility will depend on the electric field and, in general, appropriate high field mobility model for GaN HEMTs should be considered.

Saturation effects in the model are incorporated by using the saturation voltage (V_{sat}) model [25], specified by

$$V_{\text{sat}} = \frac{\upsilon_{\text{sat}}(V_{g0})}{\upsilon_{\text{sat}} + \left(\frac{\mu}{2L}\right) V_{g0}}. \tag{9}$$

Here, υ_{sat} is saturation velocity (1.2×10^7 cm/s), and $V_{\text{g0}} = V_{\text{gs}}$–$V_{\text{OFF}}$, where V_{g} and V_{OFF} are the gate voltage and threshold voltage, respectively. μ is the mobility inside the channel from (7). Additional information about this model is provided in the supplementary material.

B. Compact Thermal Model

Compact thermal model is based on a thermal resistance network modeling approach in which the computational domain is divided into a number of small regions, which are represented by equivalent thermal resistances in the network (Fig. 2). Although the thermal resistance network approach for GaN HEMTs has been previously employed [26], when combined with the above-mentioned electrical model, it becomes a very useful and time-efficient technique for electrothermal co-design of GaN HEMTs. The schematic corresponds to a ten-finger AlGaN/GaN HEMT, but the methodology remains similar for any number of fingers. Thermal resistance of each cell depends on the material thermal conductivity, length of the cell, and area (width in 2-D case) of the cell normal to propagation of heat. The model allows the usage of temperature-dependent thermal conductivity for GaN ($k_{\text{GaN}} = 150\ (\text{T}/300)^{-1.4}$) and substrate ($k_{\text{Si}} = 148\ (\text{T}/300)^{-1.3}$) in the thermal model [27]. Dissipated power in the channel due to Joule heating is specified at certain nodes at the top in the network that represent the channel regions [Fig. 2(b)]. For simplicity, we consider only two layers in the 2-D thermal model: GaN (2 μm thickness) and the substrate (Si, 300 μm

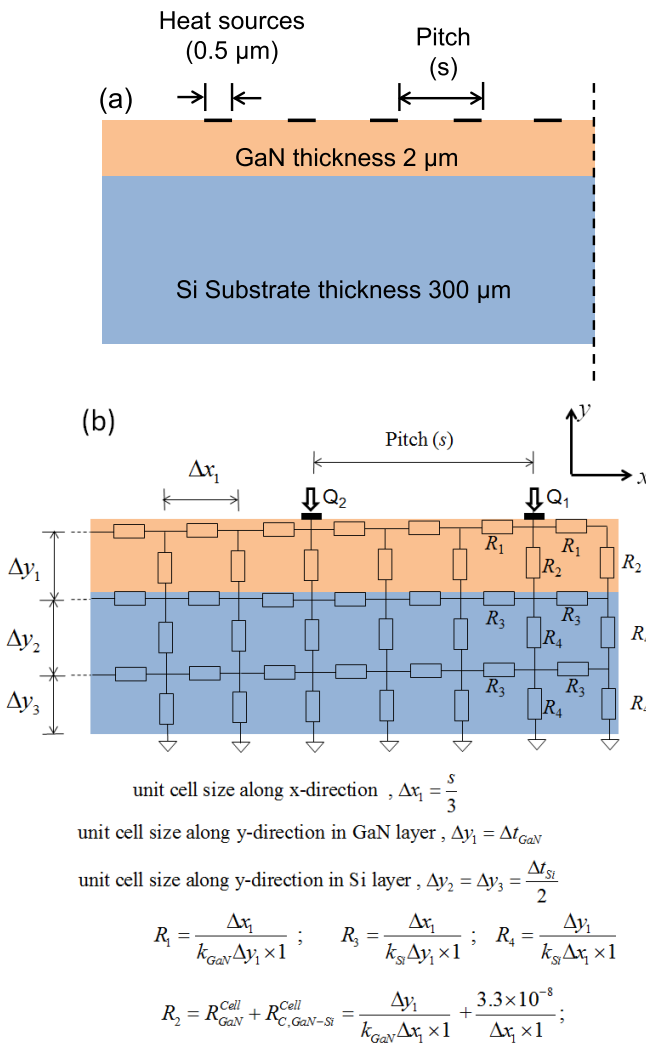

Fig. 2. (a) Schematic of the computational domain of ten-finger AlGaN/GaN HEMT used in finite-volume simulations; only half of the domain is considered due to symmetry. Heat source length is 0.5 μm, and three cases with different pitch lengths (s = 30, 40, and 50 μm) are studied. (b) Thermal resistance network used in the compact thermal model; power dissipation due to Joule heating (Q_1, Q_2 etc.) is specified into specific nodes representing the channel region in the network. Here, Δx_1 = pitch/3, $\Delta y_1 = \Delta t_{\mathrm{GaN}}$, $\Delta y_2 = \Delta y_3 = \Delta t_{\mathrm{Si}}/2$. R_1 is unit-cell thermal resistance along x-direction in GaN layer, R_2 is unit-cell thermal resistance along y-direction which includes GaN layer resistance and GaN-Si contact resistance, R_3 is unit-cell thermal resistance along x-direction in Si layer, R_4 is unit-cell thermal resistance along y-direction, in Si layer. $k_{\mathrm{GaN}} = 150\ (\mathrm{T}/300)^{-1.4}$ W/mK and $k_{\mathrm{Si}} = 148\ (\mathrm{T}/300)^{-1.3}$ W/mK are temperature-dependent thermal conductivity of GaN and Si layers, respectively. Δt_{GaN} and Δt_{Si} are thickness of GaN and Si layers, respectively.

thickness) as other layers above GaN are too thin to have any significant effect on the temperature. Thermal contact resistance at the interface between GaN and substrate is taken as 3.3×10^{-8} m^{2}K/W [1]. This is included in the thermal resistance network by adding into GaN-layer thermal resistance. The bottom of the substrate layer is considered to be at constant temperature of 300 K. Other boundaries are treated as adiabatic.

At first, the power dissipation ($Q = V_{\mathrm{ds}} \times I_{\mathrm{ds}}$) for all fingers is calculated using the drain current model at 300 K. The dissipated power (Q) is used as the input heat source at the finger nodes [Fig. 2(b)] in the thermal resistance network to obtain the temperature at all nodes. The temperature at the channel/finger nodes is utilized to update the value of temperature-dependent thermal conductivity, and the thermal resistance network is solved again. The process is repeated for self-consistency within the thermal resistance network, which is implemented by making sure that the relative change in the maximum temperature with respect to previous iteration ($|(\mathrm{Tmax, i+1} - \mathrm{Tmax, i})/\mathrm{Tmax, i}| < 10^{-3}$) is negligibly small. Subsequently, the temperature at the channel/finger nodes is then used to update the mobility and get updated current. The process is repeated for the self-consistency between the current and temperature at a given V_{gs} and V_{ds}. Thus, there are two self-consistency loops (one due to thermal conductivity, another due to mobility) involved in the overall process. Less than ten iterations are needed to achieve convergence and self-consistent solution in single-finger GaN HEMT. Here, ten iterations means that drain current model (which utilizes temperature (K) obtained from thermal model) and thermal model (which utilizes power dissipation (W) in the channel obtained from drain current model) are solved sequentially ten times. It takes less than 40 s on an Intel core i-7 processor to obtain the entire set of self-consistent I–V curves (Fig. 3). For ten-finger device simulations, we have used 20 iterations for self-consistency. It takes 3.2 s on Intel core an i-7 processor to obtain current and temperature in the ten-finger device corresponding to $V_{\mathrm{ds}} = 10$ V and $V_{\mathrm{gs}} = 1$ V. Number of iterations (and hence the computation time) needed for solutions corresponding to lower values of V_{gs} will be smaller as temperature effects will be smaller. Both electrical and thermal models are implemented in MATLAB. Gauss–Seidel method is used to solve for temperature from the thermal resistance network.

III. Results and Discussion

A. Single-Finger AlGaN/GaN HEMT

For the purpose of validation of the compact electrothermal model, we obtain the experimental data from literature [1] for AlGaN/GaN HEMT device as shown in Fig. 1. Here, the gate length, gate-to-source spacing, and gate-to-drain spacing are 2, 1.5, and 3 μm, respectively. Thickness of SiN, AlGaN, GaN, and Si layers are 50, 20, 2, and 300 μm, respectively. Fig. 3(a) shows comparison of the output characteristics from the experiments and the corresponding single-finger AlGaN/GaN HEMT compact electrothermal model. We find that the results obtained from the self-consistent model agree well with the experiments. It can be noted here that the self-heating effects become very significant for higher gate bias values, which leads to negative differential resistance in the saturation region. These effects are well captured by the compact electrothermal model underlining its predictive ability [see Fig. 3(a)] and confirming its validity. Fig. 3(b) shows the results of channel temperature variation at different bias conditions obtained using the compact electrothermal model of the single-finger AlGaN/GaN HEMT. Higher gate bias leads to greater current in the channel, which results in higher power dissipation and subsequently higher temperature.

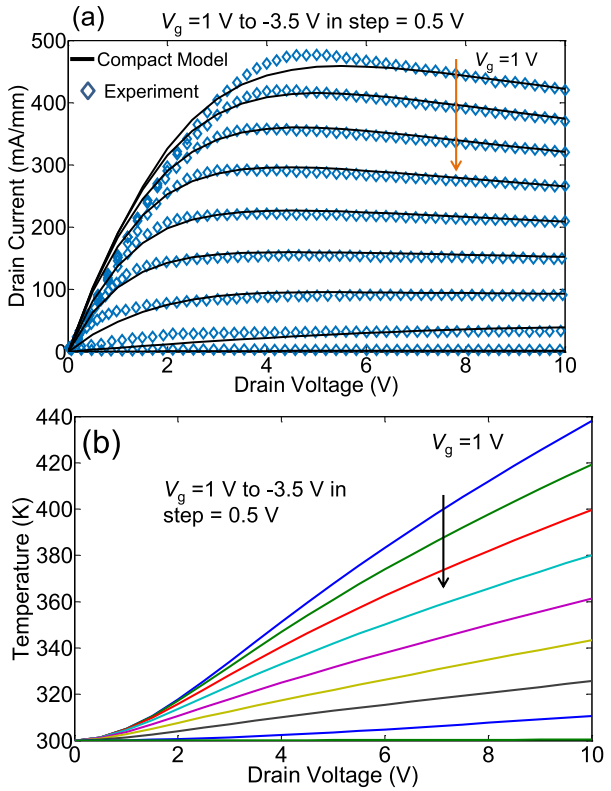

Fig. 3. (a) Comparison of output characteristics of GaN HEMT from experiments [1] and compact electrothermal model. (b) Temperature variation with drain voltage for different gate voltages. Gate voltage (V_g) is varied from 1 to −3.5 V in the steps of 0.5 V.

The computational domain for the device is shown in Fig. 1. For simplicity, we consider only two layers in the thermal model: GaN (2 μm thickness) and the substrate (Si or SiC, 300 μm thickness) as other layers above GaN are too thin to have any significant effect on the temperature. Thermal contact resistance at the interface between GaN and substrate (3.3×10^{-8} m^{2}K/W) has been included [28]. Temperature-dependent thermal conductivity has been used for all the materials, and the mathematical expressions for each are mentioned earlier. Heat source is considered to be 0.5 μm with 50 μm lateral width for thermal spreading on either side. The bottom of the substrate layer is considered to be at constant temperature of 300 K. Other boundaries are treated as adiabatic. Fig. 4 shows the channel temperature variation against dissipated power with constant and temperature-dependent thermal conductivity. It is clear that for higher power (>1 W/mm), the effect of temperature dependence on thermal conductivity starts showing on the temperature profile such that this effect becomes more dominant with increasing power. This shows that the temperature dependence of thermal conductivity is very important in predicting the correct electrothermal transport characteristics for AlGaN/GaN HEMTs, considering the fact that these devices are potential candidates for higher power applications.

B. Multifinger AlGaN/GaN HEMT

1) Passive Cooling: To further demonstrate the utility of the compact electrothermal model in the case of multifinger

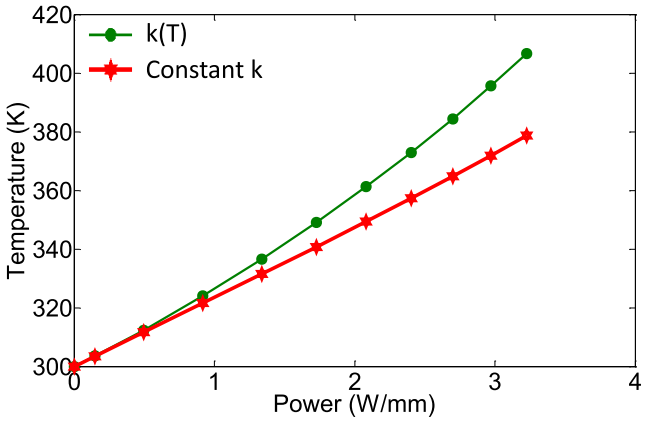

Fig. 4. Effect of temperature dependence of thermal conductivity on the temperature variation with power dissipation in single-finger AlGaN/GaN HEMTs. Results indicate that it is important to consider the temperature dependence of the thermal conductivity particularly at high power.

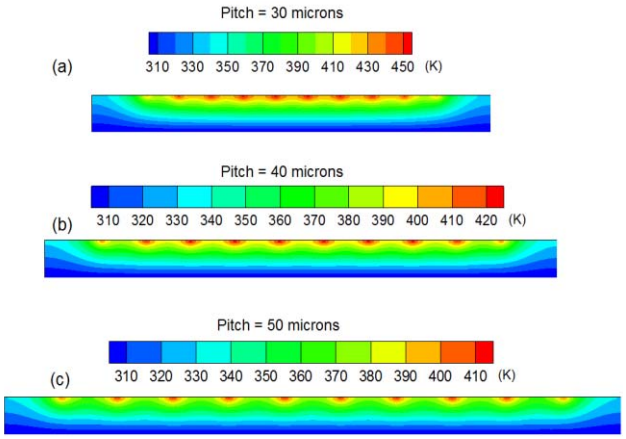

Fig. 5. 2-D temperature contour plots of multifinger GaN HEMT for different pitch length (a) 30, (b) 40, and (c) 50 μm. Lower pitch length leads to lower lateral thermal spreading and higher thermal crosstalk among the heat-dissipating channel regions, which results in higher temperature. Results correspond to gate voltage $V_g = 0$ V and drain voltage $V_d = 10$ V.

HEMTs, we consider a ten-finger AlGaN/GaN HEMT with Si substrate. 2-D thermal simulations are carried out for the ten-finger device. The results for temperature profile in the device obtained from finite-volume thermal simulations are shown in Fig. 5. We study cases of three different finger-to-finger spacings referred to as pitch length ($s = 30$, 40, and 50 μm). Here, we assume the length of the heat source to be 0.5 μm for each finger.

Results in Fig. 5 illustrate the effects of self-heating, thermal spreading, and thermal "coupling" or "crosstalk" among fingers on the temperature profile. The temperature profile shows local maxima at the location of heat sources. We can note that the higher pitch length leads to better lateral thermal spreading and lower thermal crosstalk effects, which lowers the peak temperature in the device as seen in [1], [29]. Also, we observe that temperature is significantly lower for the outermost fingers compared to the inner ones due to the same reasons.

We compare the temperature results (Fig. 6) obtained from compact electrothermal model and finite-volume thermal simulations to illustrate the capability of the model for

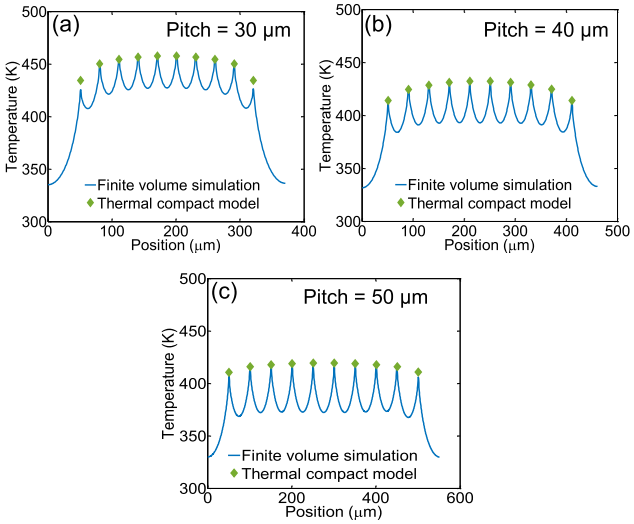

Fig. 6. Temperature variation along the lateral direction in multifinger GaN HEMT at gate voltage, $V_g = 0$ V and drain voltage $V_d = 10$ V for three different pitch lengths (a) 30 μm, (b) 40 μm, and (c) 50 μm. Solid curves and symbols represent results from finite-volume thermal simulations and thermal compact models, respectively. Results underline the validity of the compact model.

temperature prediction with reasonable accuracy. The figure shows the spatial variability in the temperature profile in the lateral direction at the top surface of a ten-finger GaN HEMT for three different pitch lengths. Here, we note that as the pitch decreases from 50 to 30 μm, the peak temperature in the device increases by 35 °C. The temperatures at inner fingers are nearly identical. However, they drop appreciably for the outermost fingers. This drop increases from 15 °C to 35 °C as the pitch decreases from 50 to 30 μm. Overall, we find that the results from the compact model agree well with the results of finite-volume-based thermal simulations. With the combined benefits of significantly reduced computation time and reasonable accuracy, the presented compact electrothermal model can serve as a very useful and cost-effective tool for design and analysis of GaN-HEMTs based circuits.

2) Microchannel Cooling: In order to perform self-consistent electrothermal modeling of microchannel cooling, we combine electrical dc model discussed earlier with CFD model of AlGaN/GaN using ANSYS Fluent (Fig. 7). We consider the full 3-D model of the device for the CFD calculations with dimensions and material properties specified in [1]. Die area of the device is considered to be 650 × 650 μm^2. The heat flux area corresponding to each finger is 0.5 × 250 μm^2. The pitch between gate fingers is 50 μm. The die (2-μm GaN buffer layer on 300-μm-thick Si substrate) is considered to be attached to CuW (640 μm) package with a 50-μm-thick AuSn solder layer. The package is considered to be mounted on a heat sink (a copper cold plate) using a 50-μm-thick thermal epoxy layer. Water-glycol mixture is used as the coolant for microfluidics cooling with four microchannels embedded in Si substrate each of 100 × 100 μm^2 cross-sectional area. A total of 1.3 million cells have been used in the CFD model after performing grid independent tests. We vary the coolant flow rate between 2 and 48 mL/min.

We consider the device to be operating at $V_{gs} = 0$ V and $V_{ds} = 10$ V, and the subsequent analysis corresponds to this

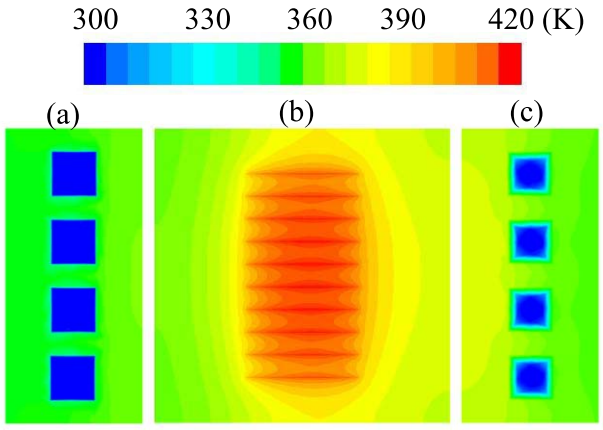

Fig. 7. Self-consistent temperature profile of ten-finger GaN on Si HEMT with embedded microchannel cooling in the Si substrate. (a) front/inlet view, (b) top view, and (c) back/outlet view. Here, $V_g = 0$ V and drain voltage $V_d = 10$ V. Total area of the device 650 × 650 μm^2. Microchannel area 100 × 100 μm^2. Each heat flux area = 0.5 × 250 μm^2. Gate finger pitch = 50 μm.

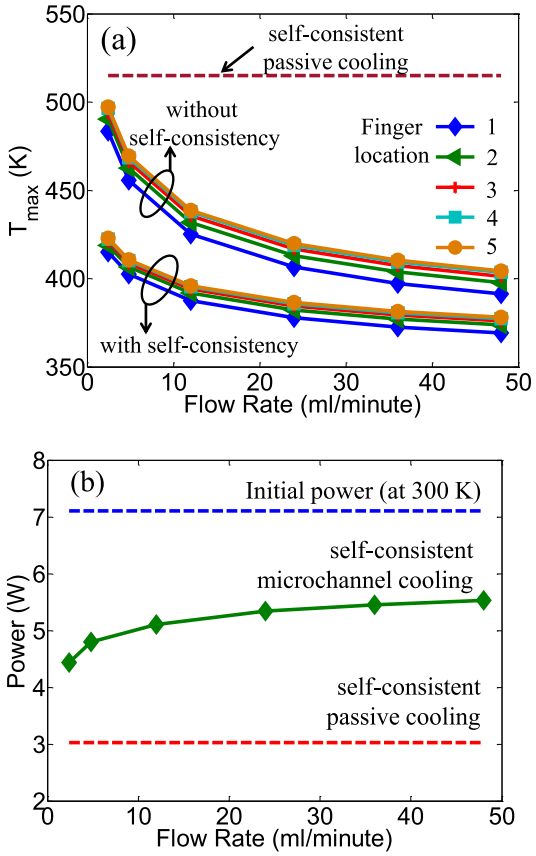

Fig. 8. (a) Variation of peak temperature of gate finger locations at varied flow rate. It also compares the effect of passive and microchannel cooling on the peak temperature. The marked effect of self-consistency in electrothermal modeling of microchannel cooling can also be seen here. (b) Variation of total power in the ten-finger device at varied flow rate. It also compares the effect of self-consistency on power [$= I_d(V_{ds}, V_{gs}, T) \times V_d$] for both passive and microchannel cooling. The blue and red dotted lines show the power in the device at $V_{ds} = 10$ V and $V_{gs} = 0$ V for isothermal and self-consistent simulations, respectively, for the case of passive cooling.

bias condition. Fig. 8 shows the peak temperature variation of gate fingers corresponding to different microchannel flow rates, and also highlights the importance of self-consistency

during the electrothermal modeling of AlGaN/GaN devices. The electrothermal simulations are run iteratively to achieve a self-consistent solution for current (power) and temperature for fixed bias voltages (V_{ds} = 10 V and V_{gs} = 0 V). We find that when the total 3 W of power is dissipated in the ten-finger device, the self-consistent peak temperature is 515 K in passive cooling. In comparison, it should be noted that the isothermal (300 K) power for the same case is nearly 7 W. With microchannel cooling, the peak temperature decreases with the increasing flow rate albeit with diminishing returns. We find significant reduction in the peak temperature ($\sim$140 K) due to microchannel cooling at the flow rate of 48 mL/min. Here, the difference in the peak temperature with and without self-consistency is about 75 K at 2.4 mL/min, and it reduces 25 K at 48 mL/min. Thus, although the self-consistency effects become smaller for higher flow rates, they remain significant for the entire range of flow rate considered here. Self-consistency effect reduces the power from 7 to 3 W in the passive cooling case. In the case of microchannel cooling, self-consistency effect on power dissipation decreases with increased flow rate as we can see that the self-consistency effect reduces the power from 7 to 4.4 W at 2.4 mL/min and to 5.4 W at 48 mL/min. It is also worth noting that the self-consistency effects are more pronounced in the passive cooling case due to higher temperature. The results discussed here clearly indicate that the accuracy of thermal design and analysis of AlGaN/GaN HEMTs-based devices will be greatly improved when thermal models are properly coupled with the electrical device models.

IV. Conclusion

We present a self-consistent electrothermal model to study the passive and active cooling in multifinger AlGaN/ GaN HEMT. In this process, we utilize a physics-based electrical compact model of the device and couple it with 2-D and 3-D CFD-based thermal models. In the case of passive cooling, we also develop a compact electrothermal model that is computationally very efficient and provides high-fidelity results. We further examine the importance of self-consistency in these models and find that the predictive capability of the "standalone" thermal models of AlGaN/GaN HEMTs can be very limited unless they are self-consistently coupled with the electrical models due to the temperature dependence of the electrical current. Comparison of active and passive cooling in these devices suggests that the device-level microchannel cooling can be very beneficial for relatively lower-thermal-conductivity substrates and self-consistent models are needed for accurate estimations of temperature and current/power.

References

[1] X. P. Chen, F. N. Donmezer, S. Kumar, and S. Graham, "A numerical study on comparing the active and passive cooling of AlGaN/GaN HEMTs," *IEEE Trans. Electron Devices*, vol. 61, no. 12, pp. 4056–4061, Dec. 2014.

[2] R. S. Pengelly, S. M. Wood, J. W. Milligan, S. T. Sheppard, and W. L. Pribble, "A review of GaN on SiC high electron-mobility power transistors and MMICs," *IEEE Trans. Microw. Theory Techn.*, vol. 60, no. 6, pp. 1764–1783, Jun. 2012.

[3] U. K. Mishra, P. Parikh, and Y.-F. Wu, "AlGaN/GaN HEMTs—An overview of device operation and applications," *Proc. IEEE*, vol. 90, no. 6, pp. 1022–1031, Jun. 2002.

[4] F. Yamaki, K. Inoue, N. Ui, A. Kawano, and S. Sano, "A 65 % drain efficiency GaN HEMT with 200 W peak power for 20 V to 65 V envelope tracking base station amplifier," in *IEEE MTT-S Int. Microw. Symp. Dig.*, Jun. 2011, pp. 1–4.

[5] A. K. Agrawal and E. L. Holzman, "Beamformer architectures for active phased-array radar antennas," *IEEE Trans. Antennas Propag.*, vol. 47, no. 3, pp. 432–442, Mar. 1999.

[6] R. T. Kemerley, H. B. Wallace, and M. N. Yoder, "Impact of wide bandgap microwave devices on DoD systems," *Proc. IEEE*, vol. 90, no. 6, pp. 1059–1064, Jun. 2002.

[7] J. Park, D. Kakovitch, M. W. Shin, and C. C. Lee, "Thermal modeling and measurement of AlGaN/GaN FETs built on sapphire and SiC substrates," in *Proc. 53rd Electron. Compon. Technol. Conf.*, May 2003, pp. 438–442.

[8] F. Bertoluzza, N. Delmonte, and R. Menozzi, "Three-dimensional finite-element thermal simulation of GaN-based HEMTs," *Microelectron. Rel.*, vol. 49, no. 5, pp. 468–473, May 2009.

[9] S. G. Kandlikar and W. J. Grande, "Evaluation of single phase flow in microchannels for high heat flux chip cooling—Thermohydraulic performance enhancement and fabrication technology," *Heat Transf. Eng.*, vol. 25, pp. 5–16, Dec. 2004.

[10] A. Bar-Cohen, J. J. Maurer, and A. Sivananthan, "Near-junction microfluidic thermal management of RF power amplifiers," in *Proc. IEEE Int. Conf. Microw., Commun., Antennas Electron. Syst. (COMCAS)*, Nov. 2015, pp. 1–8.

[11] Z. M. Lu *et al.*, "Design and modeling of membrane-based evaporative cooling devices for thermal management of high heat fluxes," *IEEE Trans. Compon., Packag., Manuf. Technol.*, vol. 6, no. 7, pp. 1058–1067, Jul. 2016.

[12] H. Lee *et al.*, "Thermal modeling of extreme heat flux microchannel coolers for GaN-on-SiC semiconductor devices," *J. Electron. Packag.*, vol. 138, no. 1, p. 010907, Mar. 2016.

[13] Y. Won, J. Cho, D. Agonafer, M. Asheghi, and K. E. Goodson, "Fundamental cooling limits for high power density gallium nitride electronics," *IEEE Trans. Compon., Packag., Manuf. Technol.*, vol. 5, no. 6, pp. 737–744, Jun. 2015.

[14] T. Y. Liu *et al.*, "Full scale simulation of an integrated monolithic heat sink for thermal management of a high power density Gan-Sic chip," in *Proc. Int. Tech. Conf. Exhibit. Packag. Integr. Electron. Photon. Microsyst.*, vol. 1, 2015, p. V001T09A057.

[15] D. H. Altman, A. Gupta, and M. Tyhach, "Development of a diamond microfluidics-based intra-chip cooling technology for gan," in *Proc. Int. Tech. Conf. Exhibit. Packag. Integr. Electron. Photon. Microsyst.*, vol. 3. 2015, p. V001T09A057.

[16] M. Garven and J. P. Calame, "Simulation and optimization of gate temperatures in GaN-on-SiC monolithic microwave integrated circuits," *IEEE Trans. Compon. Packag. Technol.*, vol. 32, no. 1, pp. 63–72, Mar. 2009.

[17] F. Bonani, V. Camarchia, F. Cappelluti, S. D. Guerrieri, G. Ghione, and M. Pirola, "When self-consistency makes a difference," *IEEE Microw. Mag.*, vol. 9, no. 5, pp. 81–89, Oct. 2008.

[18] E. R. Heller and A. Crespo, "Electro-thermal modeling of multifinger AlGaN/GaN HEMT device operation including thermal substrate effects," *Microelectron. Rel.*, vol. 48, no. 1, pp. 45–50, Jan. 2008.

[19] M. P. Gupta, A. Vallabhaneni, and S. Kumar, "A self-consistent reduced order model for current and temperature in GaN HEMTs," in *Proc. IEEE ITHERM*, Orlando, FL, USA, 2017.

[20] F. M. Yigletu, S. Khandelwal, T. A. Fjeldly, and B. Iñiguez, "Compact charge-based physical models for current and capacitances in AlGaN/GaN HEMTs," *IEEE Trans. Electron Devices*, vol. 60, no. 11, pp. 3746–3752, Nov. 2013.

[21] S. Khandelwal and T. A. Fjeldly, "A physics based compact model of *I–V* and *C–V* characteristics in AlGaN/GaN HEMT devices," *Solid-State Electron.*, vol. 76, pp. 60–66, Oct. 2012.

[22] S. Khandelwal, N. Goyal, and T. A. Fjeldly, "A physics-based analytical model for 2DEG charge density in AlGaN/GaN HEMT devices," *IEEE Trans. Electron Devices*, vol. 58, no. 10, pp. 3622–3625, Oct. 2011.

[23] D. Delagebeaudeuf and N. T. Linh, "Metal-(n) AlGaAs-GaAs two-dimensional electron gas FET," *IEEE Trans. Electron Devices*, vol. 29, no. 6, pp. 955–960, Jun. 1982.

[24] S. Kola, J. M. Golio, and G. N. Maracas, "An analytical expression for Fermi level versus sheet carrier concentration for HEMT modeling," *IEEE Electron Device Lett.*, vol. 9, no. 3, pp. 136–138, Mar. 1988.

[25] F. Schwierz, "An electron mobility model for wurtzite GaN," *Solid-State Electron.*, vol. 49, no. 6, pp. 889–895, Jun. 2005.

[26] X. Jianfeng, Y. Wen-Yan, and M. Junfa, "Numerical investigation on thermal characteristics of GaN HFETs for high power applications," in *Proc. Asia–Pacific Microw. Conf.*, Dec. 2006, pp. 433–436.
[27] B. Iñguez and E. G. Moreno, "An improved C∞-continuous small-geometry MOSFET modeling for analog applications," *Analog Integr. Circuits Signal Process.*, vol. 13, no. 3, pp. 241–259.
[28] Y. Zhang *et al.*, "Electrothermal simulation and thermal performance study of GaN vertical and lateral power transistors," *IEEE Trans. Electron Devices*, vol. 60, no. 7, pp. 2224–2230, Jul. 2013.
[29] A. M. Darwish, A. J. Bayba, and H. A. Hung, "Thermal resistance calculation of AlGaN-GaN devices," *IEEE Trans. Microw. Theory Techn.*, vol. 52, no. 11, pp. 2611–2620, Nov. 2004.

Man Prakash Gupta received the B.Tech. and M.Tech. degrees in mechanical engineering from IIT Kanpur, Kanpur, India, in 2009, and the Ph.D. and Post-Doctoral degrees in mechanical engineering from the Georgia Institute of Technology, Atlanta, GA, USA, in 2014 and 2016, respectively.

His current research interests include electronics cooling and electrothermal modeling and simulation of electronic materials and devices for both low and high power applications.

Dr. Gupta received the Best Paper Award from the IEEE and Best Poster Awards from ASME. He was a recipient of Sigma Xi Best Ph.D. Thesis Award, Georgia Institute of Technology.

Ajit Kumar Vallabhaneni received the B.E. degree in mechanical engineering from the Birla Institute of Science and Technology, Pilani, India, in 2008, the Ph.D. degree in mechanical engineering from Purdue University, West Lafayette, IN, USA, in 2014, and the Post-Doctoral degree from the Georgia Institute of Technology, Atlanta, GA, USA, in 2016.

His current research interests include multiscale thermal modeling using various computational techniques.

Satish Kumar received the M.S. degree in electrical and computer engineering and the Ph.D. degree in mechanical engineering from Purdue University, West Lafayette, IN, USA, in 2007.

He was with the Systems and Technology Group, IBM Corporation, Austin, TX, in 2008, he was responsible for the thermal management of electronics devices. He is currently an Associate Professor with the George W. Woodruff School of Mechanical Engineering, Georgia Institute of Technology, Atlanta, GA, USA. He has authored or coauthored over 90 journal or conference publications. His current research interests include thermal management, thermo-electric coolers, electrothermal transport in 2-D materials, carbon nano-structures, and their nano-electronic devices.

Dr. Kumar was a recipient of the Sigma Xi Young Faculty Award and the DARPA Young Faculty Award, and also he received the Summer Faculty Fellowship from the Air Force Research Labs, the Woodruff School Teaching Fellowship, the Purdue Research Foundation Fellowship, and a Best Paper Award from the IEEE.